COMMUNICATION

Modulating Water-Responsive Actuation Energy of Regenerated Silk Fibroin via Tyrosine Modification

Received 00th January 20xx,
Accepted 00th January 20xx

DOI: 10.1039/x0xx00000x

Maheen K. Khan,[ab] Vignesh Athiyarath,[a] Darjan Podbevšek,[a] Yeojin Jung,[ab] Seungri Kim,[ab] Yuchen Zhang,[ab] Gonca Kilavus-Ecker,[c] Raymond S. Tu,[b] and Xi Chen*[abd]

Water-responsive actuation energy density of regenerated silk fibroin is doubled through tyrosine residue modification, increasing from 1.6 MJ m^{-3} to 3.5 MJ m^{-3}. FTIR spectroscopy showed the modification results in a higher proportion of mobile water, suggesting that water-responsive performance of regenerated silk is highly sensitive to the properties of confined water and that tyrosine residue modification could serve as a scalable method for developing silk-based WR actuators.

Water-responsive (WR) materials expand and contract powerfully in response to changes in environmental relative humidity (RH). In nature, these materials serve many important functions for plants[1–3], including pinecone scales that open to release their seeds[4,5], horsetail spore elaters that curl and uncurl to allow them to walk and jump for efficient dispersal[6], and filaree seed awns that twist and untwist to burrow them into the ground[7,8]. In the past decade, many synthetic[9–13] and bio-based[14–16] WR materials have been developed and used for programmable actuators[17–23], sensors[21] and evaporation energy harvesting devices[24–26], making them useful for applications in soft robotics, sensing, and the production of clean renewable evaporation energy. Despite the recent developments in WR materials, those designed by nature still outperform synthetic alternatives[27], and the lack of complete understanding of these natural designs limits the development of more powerful WR materials and their implementation in practical applications.

[a] *Advanced Science Research Center (ASRC) at the Graduate Center, City University of New York, 85 St Nicholas Terrace, New York, NY 10031, USA*
[b] *Department of Chemical Engineering, The City College of New York, 160 Convent Avenue, New York, NY, 10031, USA*
[c] *Department of Mechanical Engineering, The City College of New York, 160 Convent Avenue, New York, NY, 10031, USA*
[d] *PhD Program in Chemistry and Physics, The Graduate Center of the City University of New York, 365 Fifth Avenue, New York, NY, 10016, USA*

Supplementary Information available: (1) Water-responsive energy density calculation, (2) Calculation of modification degree of tyrosine residues, (3) ^{1}H NMR spectra, and (4) FTIR amide I peak deconvolution.
See DOI: 10.1039/x0xx00000x

Regenerated silk fibroin (RSF) is a proteinaceous high-performance WR material that offers an ideal platform for studying the design criteria of WR actuation, due to its amenability to both physical[28,29] and chemical modification[30,31]. It is affordable, widely available, and can be fabricated into continuous sheets or fibers, allowing it to facilitate the scale up and wide-spread application of WR materials. RSF is extracted from Bombyx mori silkworm cocoons and is composed of crystalline and amorphous domains. The stiff crystalline domains are formed by a heavy chain with repeating amino acid motifs that facilitate β-sheet formation, while the flexible amorphous domains are comprised of a light chain, linked to the heavy chain by a disulfide bond; and a glycoprotein, both of which contain nonrepetitive sequences[30].

Previous studies demonstrated that increasing RSF's β-sheet crystallinity via methanol treatment increased its WR energy density, from 0.2 MJ m^{-3} to 1.6 MJ m^{-3}[32], and that there is a critical ratio of bound and mobile water that provides a threshold for WR force exertion[33], illustrating the important role of both the structure of the RSF material and its confined water. RSF's WR performance has been shown to be further enhanced by modifying these properties through the inclusion of stiff silica nanoparticles[34], and the modification of the pore structure using poly(ethylene oxide) as a sacrificial porogen[35]. This inspires us to investigate the possibility of improving its WR behavior by tuning the properties of its confined water though surface chemistry modification[36].

A variety of chemical modifications could be used to enhance interactions between water and RSF, resulting in changes to water properties. These include cyanuric chloride-activated coupling to attach poly(ethylene-glycol) molecules to RSF's tyrosine residues[37], sulfation of RSF's tyrosine and serine residues[38], and carboxylation which modifies RSF's hydroxyl and amine containing residues[39]. In this study, we employed

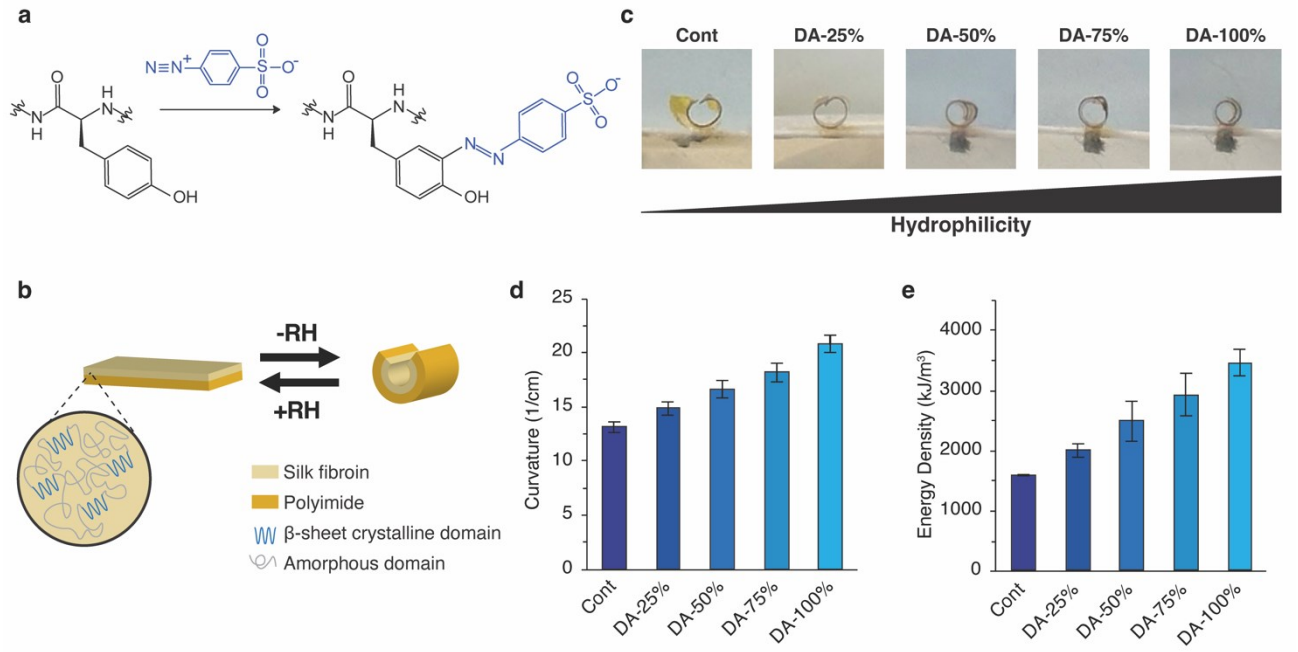

Figure 1. a) Diazonium coupling reaction between tyrosine residues of RSF and sulfanilic acid derived diazonium salt. b) Bilayer films of RSF on polyimide films curl and uncurl upon exposure to dry and humid air, respectively. c) Increasing hydrophilicity results in increased curvature of bilayer films. d) Difference in curvature of bilayer films between dry and humid state and e) difference in WR energy density of bilayer films between dry and humid state (n=5). Both increase with increasing modifications. (Error bars represent standard error).

diazonium coupling with an aniline derivative sulfanilic acid, which modifies the tyrosine residues that make up approximately 5% of RSF's total amino acid residues, without significantly affecting RSF's secondary structures. To prepare diazonium-modified RSF (DA-RSF), we varied the degree of the tyrosine residue modification by controlling the equivalents of RSF's tyrosine residues to diazonium salt, ranging from 1:0 up to 1:1. These modifications led to changes in hydrophilicity and water-material interactions, demonstrated by a 19˚ decrease in water contact angle (WCA), and a 39% increase in maximum percent water adsorption by mass. This enhanced hydrophilicity resulted in a significant increase in WR actuation energy density from 1.6 MJ m^{-3} to 3.5 MJ m^{-3}, which could be attributed to the changes in the properties of confined water.

An aqueous RSF solution was prepared by extracting silk fibroin (SF) from *Bombyx mori* silkworm cocoons (TTSAM, Amazon). Five grams of raw silk cocoons were cut into small pieces and boiled in a 0.02 M sodium carbonate (Sigma-Aldrich) solution for 30 min to remove the glue-like sericin protein. The SF was then rinsed in ultrapure water (Advantage A10, Milli-Q) three times for 20 min before being air dried overnight. 0.5 grams of silk fibroin were dissolved in 2 mL of a 9.3 M lithium bromide (Fisherbrand) solution at 60˚C for 2 hours, transferred to hydrated dialysis membrane tubing (Spectrum 3.5 kDa MWCO) and dialyzed against 400 mL ultrapure water for 2 hours, changing the water every 30 min. Finally, this solution was centrifuged at 9000 rpm (5804, Eppendorf) for 20 min, yielding a 9-10 wt% aqueous RSF solution.

The diazonium coupling reaction was performed in the aqueous RSF solution using a method reported by Hausken et al.[40], and resulted in the addition of a hydrophilic charged sulfonate group to RSF's tyrosine residues[40] (Figure 1a). The RSF solution was dialyzed against a saline borate buffer solution (9-9.5 pH, 100 mM borate buffer packs from ThermoFisher Scientific, 150 mM sodium chloride from Sigma-Aldrich) overnight followed by an additional 8 hours (24 hours total). Afterwards, this solution was diluted with saline borate buffer solution to achieve a 3% w/v RSF in saline borate buffer. Samples were prepared with the following equivalents of RSF tyrosine residues to diazonium salt to achieve varying degrees of hydrophilicity: 1:0 (DA-0%) 1:0.25 ((DA-25%), 1:0.5 (DA-50%), 1:0.75 (DA-75%), and 1:1 (DA-100%). The diazonium salt was prepared by first combining 7.9 mg sulfanilic acid (Sigma-Aldrich) and 38.0 mg p-toluenesulfonic acid (Sigma-Aldrich) in 500 µL ultrapure water. The mixture was sonicated and cooled over ice. Subsequently, 12.5 µL of 4 M sodium nitrite (Sigma-Aldrich) was added to this solution and reacted over ice for 15 min. Simultaneously, the RSF solution was cooled over ice. For the DA-100% sample, this diazonium salt solution was added to 2 mL RSF solution and reacted over ice. The amount of diazonium salt solution was scaled for each condition, and ultrapure water was added to maintain the same total reaction volume. Following a 40-min reaction period, the solutions were transferred to hydrated membrane tubing (Spectrum 3.5kDa MWCO) and dialyzed against 125 mL ultrapure water for 24 hours, with six water changes during this time.

To assess the WR capability of DA-RSF in response to RH changes, we constructed bilayer films of DA-RSF and polyimide by depositing an 8 µm thick layer of RSF onto 3x4x0.025 mm polyimide films (CAPLINQ). Free standing films were prepared by depositing a 5 µm thick layer of DA-RSF into polypropylene containers. To ensure uniform thickness and inhibit the coffee ring effect, all films were initially dried overnight in a humid chamber (>90% RH) and finished drying in ambient conditions.

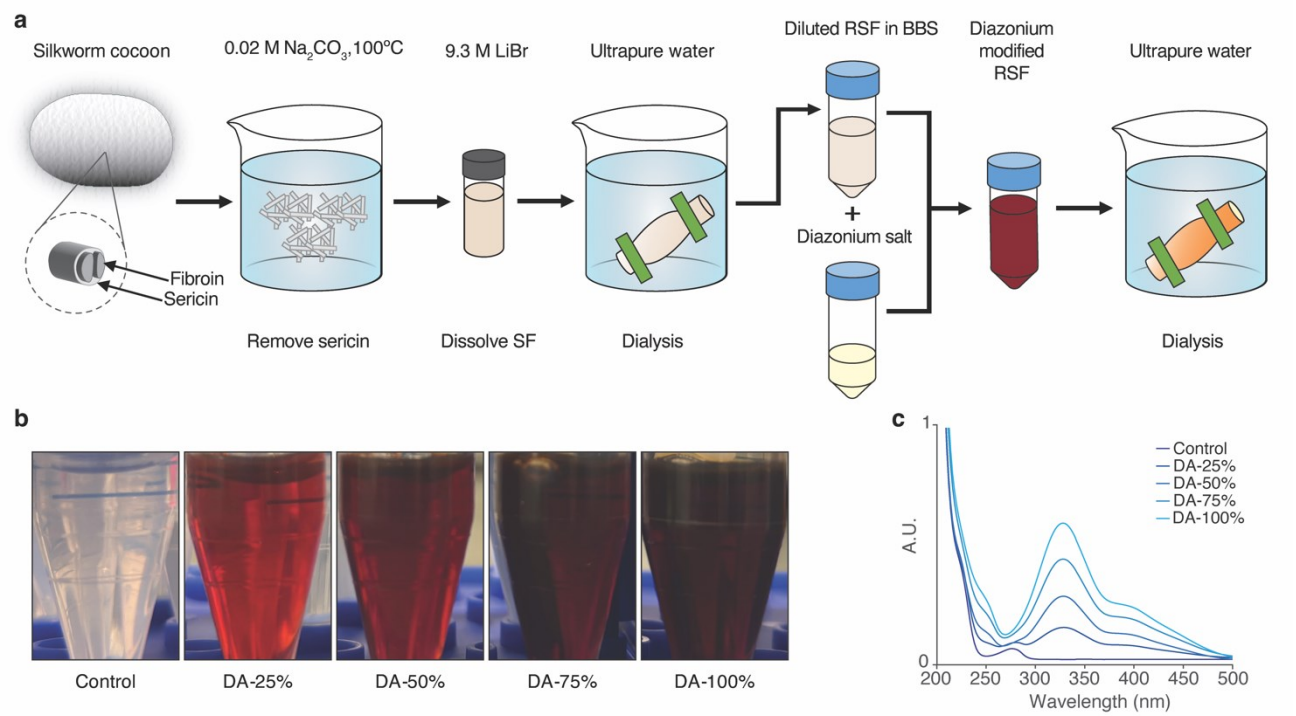

Figure 2. a) Schematic of the RSF treatment process, starting with extraction of silk fibroin from silkworm cocoons, dissolution into an aqueous solution using LiBr, dialysis against water, addition of saline borate buffer solution, reaction with diazonium salt solution, and the final dialysis against water of the modified RSF. b) Reaction solutions after 40-min reaction. The color of the RSF solutions darkens with increasing modification. c) UV-vis absorption spectra show increasing conversion with increasing ratio of diazonium salt to tyrosine residues.

The dry films were immersed in 99.9% methanol (Sigma-Aldrich) for 10 min, followed by immersion in 90% methanol for 10 min, to stabilize the β-sheet structure and ensure uniform secondary structure across all samples.

WR energy density was measured by placing bilayer films in a RH-controlled chamber, varying RH between 90% and 10% in 10-min intervals and capturing an image of the film's curvature at the end of each condition**.** The radius of curvature was measured from these images using ImageJ software. The multi-point selector tool was used to select three points along the curvature of the film, which were then fitted with a circle. The curvature was calculated as the inverse of the radius of the fitted circle. The change in curvature of the films between the dehydrated and hydrated state (Figure 1b) was used to estimate WR energy density as described previously[32]. We found that increasing hydrophilicity, by increasing the amount of modified tyrosine residues, resulted in a greater difference in curvature of bilayer films between the dehydrated and hydrated state. This difference increased from 13 cm^{-1} to 21 cm^{-1} (Figure 1c,d), and raised WR energy density from 1.6 MJ m^{-3} to 3.5 MJ m^{-3} (Figure 1e). This energy density is notably higher than that of mammalian skeletal muscles (0.8 kJ m^{-3})[41] and 17% higher than pore-enhanced RSF's WR energy density of 3.0 MJ m^{-3} [35]. These results suggest that increasing the hydrophilicity of RSF enhances its WR actuation capability and implies that tyrosine residues may play a significant role in RSF's WR behavior.

The diazonium modification results in a dramatic color change of the DA-RSF solution and gives a visual indication of the extent of modification (Figure 2a,b). The translucent nearly colorless RSF solution changed to a light amber for the DA-25% sample, darkening with increasing modification up to a deeper saffron for the DA-100% sample (Figure 2b). To further verify the modification, ultraviolet-visible (UV/vis) spectrophotometry (Jasco V-660, Spectrophotometer) was employed. The final dialyzed reaction solution was diluted to $5.47x10^{-8}$ M in 3 mL of ultrapure water and transferring to a quartz cuvette. The baseline was established with a blank of ultrapure water. Absorbance was measured between 200-550 nm wavelengths with a bandwidth of 2 nm and a data interval of 2 nm. The disappearance of the tyrosine peak around 275 nm, and appearance of a new azobenzene peak around 325 nm, that increases in intensity with increasing diazonium salt added validates the increasing modification of DA-RSF's tyrosine residues. (Figure 2b). Using Beer's law[42], we estimated the degree of tyrosine modification to be 17% for DA-25%, 33% for DA-50%, 52% for DA-75%, and 70% for DA-100% (ESI). ^{1}H nuclear magnetic resonance (NMR) further confirmed these modifications. The ^{1}H NMR (Bruker-300 Ultrashield NMR Spectrometer) spectra was obtained for DA-RSF samples dissolved in deuterium dioxide. As the degree of modification increased, the tyrosine peaks between 6.5 and 7.0 ppm increasingly broaden and shifted upfield, while new azo aromatic peaks between 7.3 and 8.0 ppm appeared downfield (ESI), consistent with previously reported ^{1}H NMR spectra for this modification[40].

The hydrophilicity of the DA-RSF was characterized using WCA measurements and water adsorption analysis. To measure the WCA, a 1 mL syringe with a 1-inch blunt needle (25GA, SANTAS) was filled with ultrapure water and clamped 2 mm above the

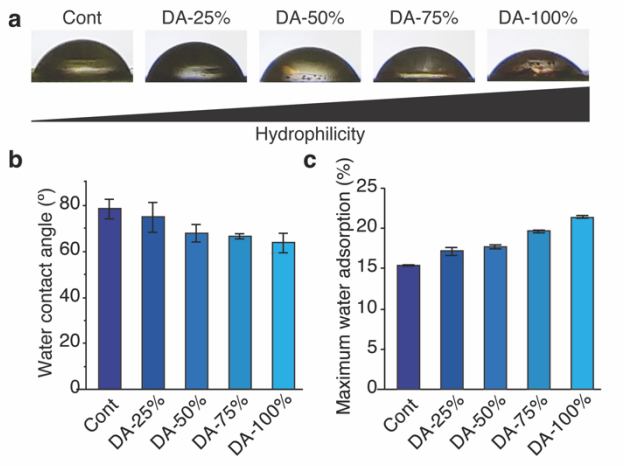

Figure 3. a) Example WCA images. b) WCA decreases with increasing modification (n=3). c) Maximum water adsorption (n=3), measured by DVS, increases with increasing modification up to DA-75%, however there is no increase seen between DA-75% and DA-100%. Error bars represent standard deviation.

bilayer films, which were flattened on glass slides. A 1.5 µL droplet was dispensed onto the surface of the bilayer film, and an image was captured 2 s after the water droplet contacted the surface. The images were analysed using the ImageJ FIJI contact angle analysis plug-in. The WCA decreased from 78˚ for the control sample to 75˚ for DA-25%, 68˚ for DA-50%, 66˚ for DA-75%, and 59˚ for DA-100% (Figure 3a,b), with in an overall decrease of 19˚. This decrease in WCA suggests that DA-RSF has increased hydrophilicity. Dynamic Vapor Sorption (DVS) (DVS Intrinsic Plus, Surface Measurement Systems) experiments were performed to measure maximum water adsorption. During this test, the RSF film was placed in a hanging sample pan attached to a microbalance. The RH inside the instrument chamber was cycled between 10% and 90% RH, for three adsorption/desorption cycles, with the end of each RH stage determined when the change in mass per time fell below 0.02 %/min for at least 10 min or for a maximum of 90 min per stage. The maximum water adsorption was obtained from the adsorption stage of the second cycle. The maximum water adsorption increased from 15% for the control sample, to 17% for DA-25%, 18% for DA-50%, and 20% for DA-75% and 21% for DA-100% (Figure 3c). Overall, the maximum water adsorption increased by only 39%, suggesting that the significant increase in WR energy density is not solely due to the addition of water to the material.

Attenuated total reflectance (ATR) Fourier transform infrared spectroscopy (FTIR) (Nicolet iS50 FTIR, Thermo Scientific) spectra were collected over a range of 400-4000 cm^{-1}, averaging 32 scans with a resolution of 4 cm^{-1} at 23˚C and 60% RH. To estimate the secondary structure of the DA-RSF films, we analysed the amide I peak between 1580 and 1730 cm^{-1} which is associated with the stretching of the backbone carbonyl bonds[43] (Figure 4a). The similarity in the shape of this peak between our control and diazonium modified samples suggests that DA-RSF's secondary structure content is similar before and after modification. To quantify the secondary structure content, the amide I peak was baseline corrected, normalized by dividing by the maximum, and fit with five Gaussian peaks representing

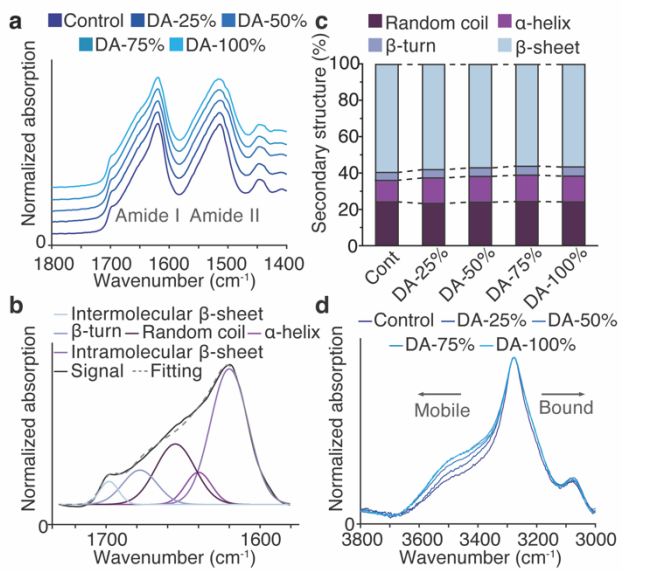

Figure 4. a) Normalized ATR-FTIR amide I and II peaks show that the control and modified samples have similar secondary structure. b) Example deconvolution of the amide I peaks for the control sample into five peaks representing intramolecular β-sheets at 1620 cm^{-1}, α-helices at 1640 cm^{-1}, random coils at 1655 cm^{-1}, β-turns at 1678 cm^{-1}, and intermolecular β-sheets at 1698 cm^{-1} c) Secondary structure content estimated from amide I peak deconvolution, combining inter- and intra-molecular β-sheets, is similar across all samples. d) Normalized ATR-FTIR OH stretching peaks at 60% RH. Arrows indicate that lower wave numbers correspond to bound water while higher numbers correspond to more mobile water.

intramolecular β-sheets at 1620 cm^{-1}, α-helices at 1640 cm^{-1}, random coils at 1655 cm^{-1}, β-turns at 1678 cm^{-1}, and intermolecular β-sheets at 1698 cm^{-1} [43] (Figure 4b). The centers of the fitted peaks were fixed and their full width at half maximum was limited between 10 and 30 cm^{-1}. The total β-sheet content was calculated by combining the areas under the intra- and intermolecular β-sheet peaks resulting in the following total β-sheet contents: 59.76% (±6.38) for the control, 58.28% (±6.36) for DA-25%, 57.23% (±4.13) for DA-50%, 56.36% (±1.48) for DA-75%, and 56.75% (±1.66) for DA-100% (Figure 4c). Overall, there is only a ~5% decrease in β-sheet content with increasing treatment, consistent with the results of previous reports using the same modification[40]. While this modification decreases RSF's propensity to form β-sheets[42], the methanol treatment may increase molecular mobility and facilitate the formation of energetically favorable β-sheets, resulting in a similar secondary structure to that of unmodified RSF[40].

We characterized the adsorbed water and the interactions between water and DA-RSF by inspecting the OH stretching peak in the ATR-FTIR spectra between 3000 cm^{-1} and 3800 cm^{-1} [44](Figure 4d). This peak was baseline correct and normalized by dividing by the maximum. In this band, lower wavenumbers correspond to bound water that has stronger hydrogen bond interactions, while higher wavenumbers correspond to mobile water with weaker hydrogen bond interactions[45]. The pronounced broadening towards higher wavenumbers suggests that there is an increase in the mobile water content, consistent with the increase in water sorption observed. Since the secondary structure of DA-RSF remains similar (Figure 4b), it is likely that the slight change in hydrogen bonding networks leads to the apparent transformation in WR properties. Previous

studies provide evidence that modest enhancement of hydrogen bonding strength in confined water[46] and hydration forces[47] could lead to a significant increase in WR pressure and energy densities, and the increase in mobile water could contribute to a rise in the total energy input during water-responsiveness[35]. It is likely that the observed two-fold increase in energy density is the combined effect of an enhanced H-bonding network resulting from increased hydrophilicity and increased water mobility.

Conclusions

The effect of increasing overall hydrophilicity of RSF through tyrosine modification on its WR properties has been demonstrated in this study. We found that modifying RSF's tyrosine residues, although they only account for about ~5% of its amino acid composition, with a hydrophilic sulfonate charged group increased its hydrophilicity, resulting in more than a two-fold increase in WR energy density from 1.6 MJ m^{-3} to 3.5 MJ m^{-3} while preserving its secondary structure. Such a significant increase in energy density is likely attributed to the increase in mobile water content and the change in the properties of confined water. This study provides a simple approach to dramatically enhance RSF's WR behavior through a small and scalable modification and enables the future design of efficient and large-scale WR actuators.

Author contributions

X.C., M.K., Y.J., and G.E. conceived and initiated the project. M.K. and Y.Z. prepared the regenerated silk. M.K. and V.A. carried out the reactions. V.A. performed NMR experiments and assisted with interpretation of the spectra. M.K. performed UV-vis, bilayer curvature, ATR-FTIR, water contact angle and DVS experiments and interpreted the results. D.P. and V.K. assisted with FTIR analysis. All authors contribute to the data analysis and the discussion of the results. M.K. and X.C. wrote the paper.

Conflicts of interest

There are no conflicts to declare.

Data availability

The data supporting this article have been included as part of the Supplementary Information.

Acknowledgements

This work was supported by the National Science Foundation (CBET-2238129). We also thank Professors Rein Ulijn and Elizabeth Biddinger for the assistance with the UV/vis and ATR-FTIR spectrometer.

References

1 C. Llorens, M. Argentina, N. Rojas, J. Westbrook, J. Dumais and X. Noblin, *The Royal Society Interface*, 2016, **13**, 20150930.
2 M. J. Harrington, K. Razghandi, F. Ditsch, L. Guiducci, M. Rueggeberg, J. W. C. Dunlop, P. Fratzl, C. Neinhuis and I. Burgert, *Nat. Commun.*, 2011, **2**, 337.
3 Z. L. Liu and X. Chen, *ACS Biomater. Sci. Eng.*, 2022, **8**, 5094–5100.
4 S. A. Khalid, P. G. Waterman, M. F. Erundan, K. B. Ch ; Anderson, R. E. Winans, R. P. Evershed, K. Jerman, G. Eglinton, J. Mills and R. White, *Nature*, 1997, **390**, 668.
5 E. Reyssat and L. Mahadevan, *J. R. Soc. Interface*, 2009, **6**, 951–956.
6 P. Marmottant, A. Ponomarenko and D. Bienaimé, *Proceedings of the Royal Society B*, 2013, **280**, 20131465.
7 D. Evangelista, S. Hotton and J. Dumais, *Journal of Experimental Biology*, 2011, **214**, 521–529.
8 A. P. C Almeida, L. Querciagrossa, P. E. S Silva, F. Gonçalves, J. P. Canejo, P. L. Almeida, ac Maria Helena Godinho and C. Zannoni, *Soft Matter*, 2019, **15**, 2838.
9 T. Wang, M. Li, H. Zhang, Y. Sun and B. Dong, *J. Mater. Chem. C*, 2018, **6**, 6416.
10 Y. Jiang, C. Hu, H. Cheng, C. Li, T. Xu, Y. Zhao, H. Shao and L. Qu, *ACS Nano*, 2016, **10**, 4735–4741.
11 Y. L. Zhang, Y. Q. Liu, D. D. Han, J. N. Ma, D. Wang, X. Bin Li and H. B. Sun, *Advanced Materials*, 2019, **31**, 1901585.
12 D.-D. Han, Y.-L. Zhang, H.-B. Jiang, H. Xia, J. Feng, Q.-D. Chen, H.-L. Xu, H.-B. Sun, D. Han, Y. Zhang, H. Jiang, H. Xia, J. Feng, Q. Chen, H. Xu and H. Sun, *Advanced Materials*, 2015, **27**, 332–338.
13 G. Jia, A. Zheng, X. Wang, L. Zhang, L. Li, C. Li, Y. Zhang and L. Cao, *Sens. Actuators B Chem*, 2021, **346**, 130507.
14 M. C. Mulakkal, R. S. Trask, V. P. Ting and A. M. Seddon, *Mater. Des.*, 2018, **160**, 108–118.
15 D. Reishofer, R. Resel, J. Sattelkow, W. J. Fischer, K. Niegelhell, T. Mohan, K. S. Kleinschek, H. Amenitsch, H. Plank, T. Tammelin, E. Kontturi and S. Spirk, *Biomacromolecules*, 2022, **23**, 1148–1157.
16 C. Lv, H. Xia, Q. Shi, G. Wang, Y.-S. Wang, Q.-D. Chen, Y.-L. Zhang, L.-Q. Liu, H.-B. C. Sun Lv, H. Xia, Q. Shi, G. Wang, Y. Wang, Q. Chen, Y. Zhang, H. Sun and L. Liu, *Adv. Mater. Interfaces*, 2017, **4**, 1601002.
17 D. Luo, A. Maheshwari, A. Danielescu, J. Li, Y. Yang, Y. Tao, L. Sun, D. K. Patel, G. Wang, S. Yang, T. Zhang and L. Yao, *Nature*, 2023, **614**, 463.
18 Y. Dong, J. Wang, X. Guo, S. Yang, M. O. Ozen, P. Chen, X. Liu, W. Du, F. Xiao, U. Demirci and B. F. Liu, *Nat. Commun.*, 2019, **10**, 1–10.
19 R. C. P. Verpaalen, M. G. Debije, C. W. M. Bastiaansen, H. Haliloví, T. A. P. Engels and A. P. H. J. Schenning, *J. Mater. Chem. A Mater.*, 2018, **6**, 17724.
20 L. Lao, H. Bai and J. Fan, *Advanced Fiber Materials*, 2023, **5**, 1076–1087.
21 Y. Zhao, Z. Yang, R. Zhou, B. Zheng, M. Chen, F. Liu, W. Miao, R. Zhou, P. Cullen, Z. Xia, L. Dai and K. (Ken) K. Ostrikov, *Journal of Bioresources and Bioproducts*, 2024, **9**, 369–378.
22 R. Pervin, P. Ghosh and M. G. Basavaraj, *Soft Matter*, 2021, **17**, 2900–2912.
23 S. L. M. Alexander and L. T. J. Korley, *Soft Matter*, 2017, **13**, 283.
24 Y. Park and X. Chen, *J. Mater. Chem. A Mater.*, 2020, **8**, 15227–15244.
25 J. Mu, C. Hou, B. Zhu, H. Wang, Y. Li and Q. Zhang, *Scientific Reports*, 2015, **5**, 1–7.
26 J. Gong, H. Lin, J. W. C. Dunlop and J. Yuan, *Advanced Materials*, 2017, **29**, 1605103.
27 H. Wang, Z. L. Liu, J. Lao, S. Zhang, R. Abzalimov, T. Wang and X. Chen, *Advanced Science*, 2022, **9**, 2104697.
28 F. Jativa and X. Zhang, *Langmuir*, 2017, **33**, 7780–7787.

29 Q. Zhang, S. Yan and M. Li, *Materials*, 2009, **2**, 2276–2295.
30 A. Reizabal, C. M. Costa, L. Pérez-Álvarez, J. L. Vilas-Vilela and S. Lanceros-Méndez, Adv Funct Mater, 2023, **33**, 2210764.
31 A. R. Murphy and D. L. Kaplan, *J. Mater. Chem.*, 2009, **19**, 6443–6450.
32 Y. Park, Y. Jung, T.-D. Li, J. Lao, R. S. Tu, X. Chen, Y. Park, Y. Jung, T. Li, R. S. Tu and X. Chen, *Macromol. Rapid. Commun.*, 2020, **41**, 1900612.
33 D. Podbevšek, Y. Jung, M. K. Khan, H. Yu, R. S. Tu and X. Chen, *Nat. Commun.*, 2024, **15**, 1–9.
34 Y. Jung, S. Sharifi Golru, T. De Li, E. J. Biddinger, R. S. Tu and X. Chen, *Soft Matter*, 2021, **17**, 7817–7821.
35 Y. Jung, M. K. Khan, D. Podbevšek, T. Sudhakar, R. S. Tu and X. Chen, *Soft Matter*, 2023, **19**, 2047–2052.
36 D. Wang, Y. Tian and L. Jiang, *Small*, 2021, **17**, 2100788.
37 Y. Gotoh, M. Tsukada, N. Minoura and Y. Imai, *Biomaterials*, 1997, **18**, 267–271.
38 Y. Tamada, *Biomaterials*, 2004, **25**, 377–383.
39 D. L. Heichel and K. A. Burke, *Bioconjug. Chem.*, 2020, **31**, 1307–1312.
40 K. G. Hausken, R. L. Frevol, K. P. Dowdle, A. N. Young, J. M. Talusig, C. C. Holbrook, B. K. Rubin and A. R. Murphy, *Macromol. Chem. Phys.*, 2022, **223**, 2200119.
41 T. Kameda, Y. Ohkawa, K. Yoshizawa, E. Nakano, T. Hiraoki, A. S. Ulrich and T. Asakura, *Macromolecules*, 1999, **32**, 8491–8495.
42 J. D. W. Madden, N. A. Vandesteeg, P. A. Anquetil, P. G. A. Madden, A. Takshi, R. Z. Pytel, S. R. Lafontaine, P. A. Wieringa and I. W. Hunter, *IEEE Journal of Oceanic Engineering*, 2004, **29**, 706–728.
43 D. J. Belton, R. Plowright, D. L. Kaplan and C. C. Perry, *Acta Biomater.*, 2018, **73**, 355–364.
44 Q. Sun, *Chem. Phys. Lett.*, 2013, **568–569**, 90–94.
45 L. Chen, X. He, H. Liu, L. Qian and S. H. Kim, *Journal of Physical Chemistry C*, 2018, **122**, 11385–11391.
46 R. Piotrowska, T. Hesketh, H. Wang, A. R. G. Martin, D. Bowering, C. Zhang, C. T. Hu, S. A. McPhee, T. Wang, Y. Park, P. Singla, T. McGlone, A. Florence, T. Tuttle, R. V. Ulijn and X. Chen, *Nat. Mater.*, 2021, **20**, 403–409.
47 S. G. Harrellson, M. S. DeLay, X. Chen, A.-H. Cavusoglu, J. Dworkin, H. A. Stone and O. Sahin, *Nature*, 2023, **619**, 500.

